Principal role of fungi in soil carbon stabilization during early pedogenesis in the high Arctic

Juan Carlos Trejos-Espeleta, Juan Marin-Jaramillo, Steven Schmidt, Pacifica Sommers, James Bradley, William Orsi

Principal role of fungi in soil carbon stabilization during early pedogenesis in the high Arctic

Juan Carlos Trejos-Espeleta[1], Juan P. Marin-Jaramillo[1,2], Steven K. Schmidt[3], Pacifica Sommers[3], James A. Bradley[4,5*], and William D. Orsi[1,6*]

[1] Department of Earth and Environmental Sciences, Paleontology & Geobiology, Ludwig-Maximilians-Universität München, Munich, Germany
[2] Current affiliation: École Polytechnique Fédérale de Lausanne, Switzerland
[3] Department of Ecology and Evolutionary Biology, University of Colorado, Boulder, CO, USA
[4] Aix Marseille University, University of Toulon, CNRS, IRD, MIO, Marseille, France
[5] Queen Mary University of London, London, UK
[6] GeoBio-Center LMU, Ludwig-Maximilians-Universität München, Munich, Germany

*Co-Corresponding authors: William Orsi, w.orsi@lrz.uni-muenchen.de; James Bradley, jbradley.earth@gmail.com

Abstract: Climate warming is causing widespread deglaciation and pioneer soil formation over glacial deposits. These pioneer soils are oligotrophic, but following initial colonization by microorganisms, accumulate organic carbon and nutrients over time. However, the mechanisms driving soil nutrient stabilization during pedogenesis remain unclear. Here we traced amino acid uptake by microorganisms in recently deglaciated high-Arctic soils and show that fungi play a critical role in the initial stabilization of the assimilated carbon. Pioneer basidiomycete yeasts were amongst the predominant taxa responsible for carbon assimilation, which were associated with overall high amino acid use efficiency and reduced respiration. In intermediate and late-stage soils, lichenized ascomycete fungi were prevalent, but bacteria increasingly dominated amino acid assimilation, with substantially decreased fungal:bacterial amino acid assimilation ratios and increased respiration. Together, these findings demonstrate that fungi are important drivers of pedogenesis in high-Arctic ecosystems that are currently subject to widespread deglaciation from global warming.

Key words: fungal ecology, stable isotope probing, Arctic soils, soil development, organic carbon.

Significance statement: Glaciers cover approximately 10% of land on Earth, yet are in rapid decline due to climate warming. As glaciers melt and retreat, they expose new bedrock and terrain that over time transforms into soil. Microbes are responsible for controlling how much carbon is stored in the newly developed soils, but how microbial activity promotes carbon storage under these conditions is poorly understood. We report that fungi in a high-Arctic glacial ecosystem drive carbon stabilization in soils within decades after glacier retreat. The pioneer fungi taxa most important for promoting carbon storage were black yeasts. Our results show that fungi will play a critical role in future Arctic soil carbon storage, as glaciers continue to shrink and expose more terrain.

Introduction: Glaciers cover approximately 10% of land on Earth, however almost all glaciers worldwide are losing mass at an accelerating rate (*1*). Climate warming is amplified in the Arctic (*2*), where glacier

retreat is particularly rapid and widespread (*3, 4*). Following ice retreat, glacial deposits undergo pedogenesis (forming proglacial soils), and retreating glacier fronts therefore provide natural laboratories where varying stages of soil development can be observed simultaneously along a chronosequence (*5-11*).

Microorganisms are the pioneer colonizers of newly exposed proglacial soils, but the microbial communities are limited by the availability of the nutrients phosphorus (P) and nitrogen (N) in the earliest stages of soil formation (*12-14*). Nutrient limited C- and N-fixing cyanobacteria and other photoautotrophs are major sources of organic C and N to the proglacial sediments and pioneer soils (*15-17*) as well as allochthonous delivery of organic C and N to the glacier forefield via glacier fed streams (*9*). As proglacial soil develops over time, organic carbon and biomass increase leading to a greater amount of stored organic C and N (9, *12-14*, *18*). Soil formation in glacier forefields exemplifies not only the carbon storage potential of newly exposed terrain, but also the recovery of soil ecosystems at the end of glacial periods and the onset of inter-glacial periods – since glacial retreat has been a consistent and widespread feature throughout Earth's past (*19*).

Bioavailable organic matter in pioneer soils of glacier forefields is subject to remineralization to CO_2 by microbial respiration - which represents an important control on how much organic C and N remains in the soil. Soil microorganisms largely control soil C storage and soil-atmosphere C exchange (*20*,*21*), and it has been proposed that microbial carbon use efficiency (CUE) is one of the key parameters controlling how much carbon is sequestered and stored in soils (*22*). CUE can be defined as the fraction of the total carbon uptake by soil microorganisms that is assimilated into biomass, versus carbon that is respired as CO_2. High CUE values are associated with high allocation of C to biomass that sequesters C as soil organic carbon (*22,23*). Natural microbial communities are complex and comprise taxa that grow and assimilate nutrients at different rates and different CUE under different conditions (*24*). Increasing the temperature of Arctic ecosystems is likely to stimulate microbial activity since many microbes live below their optimal growth temperature (*25*), but it is still poorly understood which microbes will be more or less critical for organic carbon storage under altered conditions.

Fungal traits in soil can play a key role in promoting carbon storage in soils (*26*). The ratio of fungi to bacteria, also referred to as the fungal:bacterial ratio (F:B ratio) is an important predictor of soil carbon storage because higher F:B ratios generally correspond with increased soil C storage (*27-32*). The F:B ratio is based on the fact that bacteria and fungi are two distinct and major decomposer groups in soils (32), and low F:B ratios have been found to be associated with increased respiration and decreased carbon storage capacity (29). Increased fungal activity is suggested to enhance organic C accumulation (*33*) and stabilize soil organic C via an increased CUE by fungi compared to bacteria (*28*, *30, 34*). Although fungi are prevalent in pioneer soils (*35, 36*), their role in driving carbon storage and availability during pedogenesis of glacial deposits is not known. High-Arctic ecosystems have a uniquely high diversity of fungi relative to plants (*37*), in stark contrast to low latitudes - raising the possibility that fungal communities might serve a key role as ecosystem engineers. Knowledge of carbon assimilation processes of fungal and bacterial populations and how this relates to ecosystem carbon flux is critical to understand and predict how terrestrial ecosystems in the Arctic will respond to future warming, and how they may have responded to past periods of environmental change. The magnitude and efficiency of organic carbon assimilation of individual fungal taxa and groups may indicate how they impact soil C and N storage in developing soils as Arctic temperatures rise and may also shed light on key initial stages of terrestrial ecosystem recovery after deglaciation events.

To address the role of fungi in Arctic soil development, we traced organic carbon and nitrogen uptake by microorganisms in newly exposed glacial deposits in the forefield of a retreating glacier in

Svalbard in the High-Arctic. Here, ice-free terrestrial environments are expanding at an exceptionally high rate, and these areas are subject to colonization by microbes and plants, which enhance biogeochemical cycling (*9*). We quantified fungal C assimilation by specific fungal taxa using ^{13}C labeled amino acids in quantitative stable isotope probing incubations (qSIP) of soils from three different stages of soil development along a proglacial chronosequence. DNA quantitative stable isotope probing (qSIP) is a technique that can elucidate quantitative assimilation of a given substrate by specific bacterial (*24*) and fungal (*38*) taxa. We chose amino acids as a tracer for fungal organic carbon cycling because amino acids are an important substrate for Arctic soil microbes (*39-41*). Amino acids are a major component of glacially derived dissolved organic matter (*42*) (*43*) that is delivered to the glacier forefield via glacier fed streams, and amino acid uptake and assimilation by fungi is an important control on soil carbon storage and nitrogen immobilization (*26*). In addition to fungal amino acid assimilation, we also quantified bacterial assimilation of amino acids using DNA-SIP and assessed F:B amino acid assimilation ratios. By assessing not only the F:B ratio in terms of biomass, but also F:B amino acid assimilation, we quantitatively assess how amino acid assimilation in fungi compares to bacteria at different stages of soil development. All SIP incubations were combined with measurements of ^{13}C in respired CO_2 to investigate relationships between F:B amino acid assimilation ratios and soil respiration, which provides insight into how fungal activity influences carbon cycling at different stages of ecosystem recovery and development.

Results and discussion

Soil succession in the chronosequence. The Midtre Lovénbreen chronosequence first described by Hodkinson *et al*. (*17*) proceeds from the glacier snout with several hundred meters of glacial till with no to little plant cover, followed by moraines (Fig. 1) with scattered mosses and lichens, followed by grasses and flowering plants in more mature stages of soil development. Total organic carbon (TOC), total nitrogen (TN) and total adenylate (ATP+ADP+AMP) concentrations (as a measure of total microbial biomass) was variable along the chronosequence (Fig. 2), but show a general accumulation of nutrients (TOC, TN) and microbial biomass (total adenylate) after the glacier snout (Fig. 3). Most of the increase in TOC, TN, and total adenylate was observed within the first few decades of soil formation, which is relatively stable across the remainder of the chronosequence (Fig. 2) and display increased median values in the tundra soils after the terminal moraine (Fig. 3). These trends in total biomass, TOC, and TN are largely consistent with prior observations from the Midtre Lovénbreen chronosequence showing an increase in plant cover and microbial biomass with increasing soil age (*17, 44*).

The bacterial and fungal biomass estimated by qPCR covary and correlate positively with one another across many geomorphological features throughout the proglacial soil chronosequence (Spearman Rho = 0.93, $p < 0.01$, Figs. 2 and S1a), indicating that the abundance of bacteria and fungi are tightly coupled across the entire chronosequence and both bacteria and fungi are shaped and limited by similar factors. The concentration of fungal 18S rRNA genes was consistently 1 to 2 orders of magnitude lower than the concentration of bacterial 16S rRNA genes. Fungal and bacterial biomass was lowest in the youngest soils immediately in front of the glacier (fungi: 10^6 18S rRNA gene copies g^{-1}; bacteria: 10^7 16S rRNA gene copies g^{-1}). Bacterial 16S rRNA gene abundance increased notably in the earliest stages of development, reaching a plateau in soils approximately 30 years old (at 10^9 16S rRNA gene copies g^{-1}) (Fig. 2). In contrast, fungal 18S rRNA gene abundance is slower to reach a plateau – occurring in soils ca. 50 years old (at 10^8 fungal 18S rRNA gene copies g^{-1}) (Fig. 2). After 50 years of soil development, bacterial and fungal 18S rRNA gene abundance varies across the chronosequence with intermittently lower values

until the terminal moraine but generally remains at or below the concentrations observed at 30 or 50 years of development, respectively (Fig. 2). In the older tundra soils (>120 years), located outside the terminal moraines (Fig. 1), the concentration of fungal 18S and 16S rRNA genes are relatively constant (Fig. 2). These findings are generally consistent with observations that the accumulation of nutrients in proglacial soils is accompanied by increased microbial biomass and activity (*45*, *46*).

We assessed the diversity of bacterial communities via 16S rRNA gene sequencing which showed the glacier and glacier snout communities are dominated by Gammaproteobacteria, Cyanobacteria, and Bacteroidetes, whereas the communities in the young soils directly in front of the glacier (ca. 10 years old) have a higher relative abundance of Alphaproteobacteria, and lower relative abundance of Cyanobacteria (Fig. 2d). Chloroflexi, Acidobacteria, Planctomycetes, and Actinobacteria increase in relative abundance to become dominant in 30-year-old soils. After 50 years, the major bacterial groups do not exhibit substantial changes in relative abundance, except for Chloroflexi which shows variability correlating positively with TOC (Spearman Rho = 0.556, $p < 0.001$) (Fig. 2). Overall, our results are consistent with previous surveys of this forefield (*17*) and other proglacial chronosequences (*47*, *48*).

The diversity of fungi was assessed using high-throughput sequencing of the internal transcribed spacer region 1 (ITS1), a marker for fungal taxonomic identifications (*49*), which showed that the fungal communities on the glacier and glacier snout are significantly different from the proglacial soil (ANOSIM $R = 0.9829$, $p = 0.001$) and were dominated by Microbotryomycetes (Basidiomycota) (Fig. 2d). This is consistent with general observations that glacier associated fungal communities tend to be dominated by Microbotryomycetes and other cold-adapted basidiomycete yeasts (*50-57*) that are selected for under the extremely cold conditions of the high-Arctic (*58*) possibly as a result of yeast stress-tolerance traits (*26*). The fungal community changes dramatically in the glacier snout till (site A) to become overwhelmingly dominated by taxa affiliated with the basidiomycete group Moniliellomycetes (81% of total fungal ITS reads) (Fig. 2d). The dominance of Moniliellomycetes (Basidiomycota) in proglacial sediments is constrained to site A0, 40 m from the snout of the glacier, and is consistent with basidiomycetes fungi dominating the glacier associated mud (n=3) and glacial snout (n=3) sediments immediately adjacent to this site, prior to the onset of pedogenesis. Beyond site A1, the Leotiomycetes (Ascomycota) replaces Moniliellomycetes as the dominant fungal group after only 10 years of soil development (increasing from 5% to 87%). In older soils (>30 years) the fungal community gradually becomes dominated by lichenizing groups of Eurotiomycetes (57.5 ± 26.6%) (Fig. 2d). Our observations are consistent with previous reports of stark differences between glacial (cryoconite) and soil (moraine and tundra) fungal communities (*55*) and increased fungal diversity with increasing stages of soil development (*59*). The differing rates of fungal and bacterial community assemblies seen here (Fig. 2) could be attributed to environmental filtering and selection whereby fungi and bacteria respond differently to the various physico-chemical factors along the transect (*7*,*8*), and/or that bacteria have a more cosmopolitan distribution than fungi in this particular region of Svalbard (*53*).

The fungal community appears to switch from being dominated by oligotrophic, psychrophilic basidiomycete yeasts in the glacier and proglacial sediment, towards lichenizing fungi in the more developed soils. In the early stages of soil development, the basidiomycete yeasts (Microbotryomycetes and Moniliellomycetes) that dominated the glacier and glacial snout sediments (Fig 2d) are likely sourced from supra- and subglacial environments (*60*, *61*). The Moniliellomycetes OTUs in site A and A1 are dominated by the genus *Moniliella*, a group of black yeasts, and appear to represent key pioneer fungi, that are quickly replaced by Ascomycota (Letiomycetes) within a matter of decades (Fig. 2). The transition of fungal communities in more developed soils could be explained by the development of plant root systems

(*46*), that are associated with mediation of carbon and nitrogen cycling (*62*) and increased nutrient availability (*18*). This is a likely factor explaining the increase in fungal abundance for the first several decades along the chronosequence, and the fungal community succession towards lichenizing Eurotiomycetes in the later stages of the chronosequence where soils have denser coverage of mosses and plants (*17*) (Fig. 2).

Geomorphological features along the transect were used to group the samples into the following gradient classes: glacier, snout, early soils, inner moraine, intermediate soils, terminal moraine, tundra (Figs. 1 and 2). Grouping the transect sites into gradient classes, the ratio of bacterial 16S to fungal 18S rRNA genes shows that the fungi:bacteria ratios (F:B ratios) are higher on the glacier and in the rock flour sediments at the glacier "snout", compared to the older soils of the chronosequence (Figs. 3 and S1b). Also, the median F:B ratio of the youngest section of the proglacial chronosequence is higher than the intermediate soils (Fig. 3). The elevated F:B ratios on the glacier and in the youngest proglacial sediments raises the possibility that these early successional sites may have relatively higher potential for increased carbon storage (*27-32*).

To better understand the ecological role of fungi in pioneer soil development and soil carbon cycling and stabilization, we performed DNA-SIP incubations with a mixture of seventeen ^{13}C-labeled amino acids from three sites representing initial, intermediate and developed soils (site A, B, C) (Fig. 1).

Amino acid assimilation by fungi and bacteria. Using qPCR to quantify bacterial and fungal rRNA gene distributions across density gradients (Fig. S2), we could determine buoyant density shifts, and calculate the ^{13}C-EAF of 16S and fungal 18S rRNA genes (Fig. 4). We found that fungi in the least-developed soils immediately adjacent to the retreating glacier snout (site A) had higher rates of amino acid assimilation than the fungi in older, more developed soils (sites B and C). The highest fungal ^{13}C-EAF in fungal 18S rRNA genes across the entire chronosequence was observed in the earliest pioneer soils (site A), reaching ^{13}C-EAF values >50% (Fig. 4). Here, the fungal 18S rRNA genes were labeled in all three SIP incubations tested after 7 days (median fungal EAF: 15%), including those with added kaolinite and montmorillonite (albeit 3-20 fold less compared to the control) (Fig. 4) - indicating high rates of fungal activity. At site B (inner moraine), no fungal amino acid assimilation was detected; rather bacteria were observed to assimilate amino acids in every SIP incubation at this site (Fig. 4). The dominance of bacterial amino acid assimilation over fungi at site B, may be due to an increased competition between bacteria and fungi in the intermediate soils, and that bacteria are more limited by amino acids at this site compared to fungi. In the tundra soil, fungal amino acid assimilation after 1 day was comparable to bacteria (fungal EAF: 19%, bacterial EAF: 31%), and fungal amino acid assimilation was higher than bacteria after seven days in tundra soils incubated with montmorillonite-amended amino acids (Fig. 4).

It is well known that rates of microbial amino acid assimilation in soil uptake experiments are impacted by incubation conditions, namely moisture and concentration of the added amino acids (*40*). The soils and sediments investigated here are located in a hydrologically dynamic glacial forefield that experiences large seasonal fluctuations in moisture due to precipitation and glacier fed streams (*17*) and so additional moisture in the SIP incubations was reflective of conditions that the microbes are naturally exposed to. The kinetics of amino acid uptake in soils are controlled by the concentration of amino acids added (*40*) and so the addition of amino acids probably increased rates relative to the *in situ* state at the time of sampling. To reduce excessive alteration of the system, we added the amino acids at a concentration <5% of the natural TOC concentration (Fig 2a). The concentrations of amino acids in our incubations were roughly three times lower compared to a previous study in agricultural soil that measured bacterial amino

acid assimilation with DNA-SIP (*63*). Nevertheless, for the reasons outlined above we interpret assimilation rates with caution and only consider them to be potential rates. Our results are in general agreement with other soil amino acid uptake studies showing that some soil fungi can quickly respond to local increased addition of amino acids (40).

Compared to the fungi, we found evidence of bacterial amino acid incorporation in all sites, with mean ^{13}C-EAF values (in 16S rRNA genes) of 43% at site A (including those with additional kaolinite and montmorillonite clay minerals), 9% at site B, and 11% at site C (Figs. 4 and S2). This is consistent with prior DNA-SIP studies that found that when exposed to fresh amino acid additions, many soil bacteria can assimilate ^{13}C-labeled amino acids into DNA relatively quickly (*63*, *64*).

Amino acid assimilation was dominated by fungi in the least-developed (i.e. pioneer) soils (site A), and by bacteria in intermediate and developed soils (sites B and C respectively) (Fig. 4). Bacteria had higher EAF values than fungi in most (82%, n=11) of the SIP incubations, which might be related to the fact that bacteria have a higher amino acid uptake affinity compared to fungi (40). In general, rates of $^{13}CO_2$ respiration from amino acids were highest when amino acid assimilation was dominated by bacteria rather than by fungi (Fig. 4). This suggests that fungi in early stage soils may assimilate organic carbon and nitrogen more efficiently than bacteria in later stage soils, and that the proglacial soil fungi may have higher CUE compared to bacteria. This observation fits with predictions of increased CUE by stress-tolerant yeasts adapted to extreme environments that can promote enhanced soil C storage (*26*). Our finding of higher CO_2 production rates in more developed soils is consistent with alpine proglacial ecosystems that transition from CO_2 sinks to sources with decreasing glacier coverage and an increase in vegetation (*65*).

Fungal:bacterial amino acid assimilation (EAF) ratios. In order to assess how ratios of fungal to bacterial carbon assimilation relate to respiration, we used the ^{13}C-EAF values of fungal 18S and bacterial 16S rRNA genes (Fig. 4) to calculate F:B EAF ratios. Across all of the incubations performed, at the three different successional sites, the F:B EAF ratio correlates negatively with $^{13}CO_2$ production from respiration (Fig. 5) (Spearman Rho = 0.657, $p = 0.024$, $R^2 = 0.5159$, $p = 0.005$). This shows that in the pioneer soils where fungi dominated the amino acid assimilation (relative to bacteria), there was less remineralization of organic carbon CO_2 and a higher assimilation into biomass. In contrast, when bacteria dominated amino acid assimilation (relative to fungi) there is more remineralization of organic carbon from amino acids and thus CO_2 produced. The negative correlation between respiration and F:B EAF ratio (Fig. 5) strongly suggests a higher fungal amino acid CUE and consequently increased soil carbon stabilization as biomass. Incubations from the proglacial rock flour sediments (not containing additional clay minerals) exhibited the highest F:B EAF ratios and the lowest $^{13}CO_2$ production (Fig. 5), indicating that pioneer fungi promote carbon storage and stabilization. As glacier coverage decreases, proglacial ecosystems transition from CO_2 sinks to sources (*65*) and our findings indicate that fungi play a critical role in the early stages of pedogenesis and carbon stabilization shortly after glacier retreat.

Our findings are consistent with temperate fungal-bacterial carbon turnover dynamics where increased F:B ratios also correlate with decreased respiration and increased C storage (*27*), and low F:B ratios that were associated with increased respiration and decreased carbon storage capacity (*30*). The higher F:B EAF ratios at site A (Fig 5) immediately adjacent to the snout, is consistent with higher F:B biomass ratios in the glacier and snout sediments, and the younger proglacial sediments (Fig 3). These results prompted us to investigate which fungal taxa were responsible for the high F:B EAF ratios in the pioneer soils, to establish quantitative links between key fungal taxa and carbon cycling processes.

Fungal taxon-specific amino acid assimilation. To identify the key fungal taxa responsible for amino acid cycling with qSIP, we chose the two SIP incubations that had the highest ^{13}C-EAF in fungal 18S rRNA genes from youngest (glacier snout, site A; 7-day incubation with no mineral addition) and oldest (tundra, site C; 7-day incubation with montmorillonite) sites. Due to the low fungal biomass at site A (Fig 2), the amount of extractable DNA was only sufficient for a single SIP replicate and therefore a quantitatively normalized Tag-SIP protocol ("Tag-qSIP") was performed (see Methods) to identify the labeled fungi and estimate their ^{13}C-EAF values. In the tundra soil (site C) fungal biomass was higher (Fig 2) and the amount of extractable DNA was sufficient to allow for replicates, and thus qSIP could be applied (*24*). At the tundra site (site C), there was sufficient DNA extracted to allow for multiple ultracentrifugation replicates that were used as technical replicates for qSIP. The qSIP therefore was performed as previously described (*66, 67*) on three technical replicates of density gradient fractionated DNA extracted from the tundra SIP incubations. This allowed us to assess technical variation in shifts of DNA buoyant density between labeled treatments and unlabeled controls.

The recently exposed rock flour sediments (site A0) and the more developed tundra soils (site C) differ in fungal taxon-specific amino acid assimilation (Fig. 6), both in magnitude and the identity of key active taxa. In the youngest soil (site A0), fungal OTUs exhibited on average higher EAF (52.90 ± 20.38 %), with five OTUs associated with the dominant basidiomycetes genus *Moniliella* (Moniliellomycetes) showing the highest rates of carbon assimilation (up to 100% ^{13}C EAF) (Fig. 6). The OTU clustering results of the fungal ITS1 data from the Tag-SIP incubations and chronosequence data revealed that the *Moniliella* affiliated OTUs that assimilated relatively high amounts of amino acids in the SIP incubations (Fig. 6) were the same fungal OTUs that dominated the proglacial soils at site A0 (Fig. 2d). These Moniliellomycetes affiliated OTUs corresponded to 28% and 63% of the total ITS1 sequences in the fungal community at the end of the ^{13}C-labeled amino acid and unlabeled control incubations at site A0, respectively. Notably, a single *Moniliella*-affiliated OTU with 100% ^{13}C-EAF (Fig. 6) represented 49% of the total ITS1 sequences at the end of the SIP incubations. This relatively high abundance of ^{13}C-labeled Moniliellomycetes affiliated OTUs in the ^{13}C-labeled and control SIP incubations at site A0 supports the fungal chronosequence data indicating that the Moniliellomycetes are a dominant group in the earliest proglacial soils at this site (Fig. 2).

Moniliella is a genus of basidiomycete black yeasts (*68*) that have been reported from a relatively small number of environments – predominantly human-affected ecosystems such as industrial and agricultural settings but have also been isolated from flowers in tropical rainforests (*68-70*). Our results show that a *Moniliella* sp. was the most important ecosystem engineer in the initial stages of soil development – and thus our study expands the known ecological role of this organism to including soil carbon storage in the high-Arctic. Some *Moniliella* species are considered to be xerophilic and therefore can tolerate extreme dry conditions with low water activity (*68-70*). These traits would help to explain why fungi affiliated with the *Moniliella* dominates the fungal community in the early stages of the proglacial chronosequence (Fig. 2), which experience frequent wetting and drying, as well as freeze-thaw. While psychrophilic and oligotrophic basidiomycete yeasts tend to dominate fungal communities in polar ecosystems (*51-54*), to our knowledge our results are the first reporting the ecological function of psychrophilic *Moniliella* taxa in the cryosphere.

In the Tag-qSIP results from sediments adjacent to the glacier snout (site A), several Microbotryomycetes affiliated OTUs (*Yamadamyces* sp. and *Phenoliferia* sp.) had high ^{13}C-EAF (88.8% and 31.5%, respectively). These basidiomycete yeast taxa dominated the glacier-associated fungal community but were in relatively low abundance at site A (Fig 2d) where the SIP incubation was performed

- only 40 meters from the glacier snout (Fig. 1). Their high ^{13}C-EAF (Fig. 6) compared to their low *in situ* abundance at site A (Fig. 2) indicates that their activity in proglacial sediments, after being transported from the glacier, might be limited in part by amino acids (or labile organic carbon in general).

Our results show that the ability of cold-adapted basidiomycete yeasts to assimilate amino acids is an important trait contributing to carbon stabilization in the high-Arctic ecosystem. A large number of psychrophilic yeasts and yeast-like fungi affiliated with the Microbotryomycetes have been isolated into pure culture from high-Arctic glacial environments, with some strains exhibiting dimorphic filamentous growth and rudimentary pseudohyphae (*51*). Psychrophilic Microbotryomycetes yeasts that were isolated from Arctic glacial environments were found to be able to assimilate a wide range of simple to complex sugars and polysaccharides, as well as amino acids (*51*). Melanin pigmentation is another common trait in polar basidiomycete yeasts (*71*) that may contribute to early soil carbon stabilization in proglacial soils, because melanin from fungal necromass stabilizes soil organic matter (*72*). Therefore, an increased contribution of melanin containing psychrophilic basidiomycete yeasts to the necromass carbon pool in the proglacial sediments could be an additional fungal trait promoting early soil and carbon stabilization.

In the tundra, no basidiomycete Microbotryomycetes or Moniliellomycetes fungal OTUs were found to assimilate amino acids (site C, Fig. 6) indicating that the amino acid assimilating fungi in the tundra were distinct compared to the proglacial soils. Additionally, the amino acid assimilating fungi in the tundra have on average lower ^{13}C-EAF values compared to the proglacial sediment fungal taxa and are instead dominated by Ascomycota (Sordariomycetes, Dothideomycetes, Leotiomycetes and Eurotiomycetes) (Fig. 6). The fungal OTU with the highest EAF in the tundra qSIP incubations was affiliated with the genus *Mrakia* (EAF: 22.4 ± 8.4%) (Fig. 6). Cold-adapted yeasts from the genus *Mrakia* (Tremellomycetes) are often isolated from polar and alpine cryosphere habitats (*73*), consistent with their high rates of amino acid assimilation in the tundra soils seen here. Fungi are known to have differences in amino acid uptake affinities between species (*40*), and this may explain in part the different levels of amino acid assimilation observed between fungal taxa that we observed in the qSIP results.

Influence of clay minerals on amino acid assimilation. We added clay minerals to SIP incubations at each of the three sites (Fig. 1), because sorption onto clay mineral surfaces is predicted to reduce the bioavailability of organic C and N in soils (*74*) and is hypothesized to be an important component of the global carbon cycle (*75*). In general, higher rates of $^{13}CO_2$ respiration from the labeled amino acids was observed in incubations that contained the added clay minerals compared to the controls, and the correlation of clay minerals with increased $^{13}CO_2$ respiration was most pronounced in soils where bacteria dominated amino acid assimilation (Fig. 4) and a reduced F:B ^{13}C-EAF ratio was observed (Fig. 5). Bacteria have higher amino acid uptake affinity compared to fungi, meaning that bacteria can assimilate amino acids faster at lower concentrations (*40*). If amino acid sorption onto clay minerals resulted in a lower concentration of bioavailable amino acids (*74*, *76*), bacteria may outcompete fungi leading to higher bacterial EAF values under such conditions. However, under the conditions where bacteria dominated amino acid assimilation (as opposed to fungi), it was relatively inefficient and resulted in increased amino acid remineralization and CO_2 production (Figs. 4 and 5).

Conclusions. Our study shows for the first time that fungal:bacterial carbon assimilation ratios are important for carbon stabilization in the early development phase of high-Arctic soils. Our results link basidiomycete yeasts to this process, identifying them as "pioneer fungi" that likely help in the process of stabilizing organic C in young proglacial soils. These fungi traits will become more important as glaciers

continue to retreat in the high-Arctic, and they may also have been important for the recovery of past soil ecosystems during Phanerozoic glacial-interglacial cycles.

Material and Methods

Study site and sampling. Our study focusses on the proglacial forefield of Midtre Lovénbreen, a retreating polythermal valley glacier located 5 km South-East of Ny-Ålesund, in North-West Svalbard (78°55' N, 12°45' E; Fig. 1). The annual mean air temperature at the site between 1991 and 2021 was -4.1 ± 1.3 °C with a steady increase over time, and in 2021, the sampling year, the mean annual temperature was 1.2°C above the 1991 to 2021 average (Norwegian Polar Institute). We selected three main sites of increasing distance from the glacier snout (pioneer, intermediate and tundra; sites A, B, and C respectively) for qualitative assessment of vegetation communities (*17*). These sites serve as a chronosequence representing distinct stages of soil development. We also established a transect between sites A (pioneer soil) and C (tundra) across a distance of 1.2 km in the direction of ice retreat (Fig. 1b), and collected single samples at 40 m intervals along this transect (38 sites in total). We collected surface rock flour sediment or soil (upper 2 cm, excluding conspicuous microbial mats, rocks bigger than 1 cm diameter, and dense radical systems). We also collected supraglacial sediments (muddy ice) from the glacier (ca. 50 m from the snout) in biological triplicate, and we collected rock flour from the proglacial sediments within five meters of the glacier snout in biological triplicate.

Major geomorphological features along the transect were used to group the samples into the following gradient classes: glacier, snout, early soils, inner moraine, intermediate soils, terminal moraine, and tundra (Figs 1-3). The oldest soils are at the tundra sites (sites B15 – B20 and site C) are outside the terminal moraine, and likely thousands of years old having developed since the end of the last glacial maximum at this site (Fig 1a). Inside the terminal moraine, the sampled chronosequence corresponds to approximately 120 years of exposure (*17*) after glacier retreat since the end of the Little Ice Age, represented by the terminal moraine (sites B10 – B14) (Fig. 1a). An internal moraine (sites A14 – B2) divides the forefield, and seasonal glacier fed streams also cut through the terrain (sites B8 – B10) (Figs. 1 and 2). The map of the sampling area (Fig. 1a) was created using QGIS 3.18 and published estimates of soil age (*77*), according to geographical data from the Norwegian Polar Institute.

Samples were collected into 15-mL Falcon® tubes using a spatula sterilized with 70% ethanol. With the exception of samples for incubations, samples were frozen within six hours of collection and stored at -20°C until further processing. The vegetation present at sites A, B and C and along the transect was qualitatively assessed by examining sites for the presence of various plant species using photographs and field guides (svalbardflora.no; cruise-handbook.npolar.no), in keeping with prior surveys of this chronosequence (*17*).

Total adenylate, total organic carbon (TOC), and total nitrogen (TN) measurements. As a proxy for total biomass, we measured total adenylate (ATP+ADP+AMP) concentration from all samples using the "boil and dilute" method described previously (*78*). In brief, 0.5 g of sample was mixed with 1 mL of sterile MilliQ water and incubated at 99 °C for 10 minutes. The slurry was centrifuged for 2 minutes at 13,000 RPM and total adenylate in the supernatant was measured using a luminometer with the A3 assay according to the manufacturer's instructions (A3 Lucipac, Kikkoman). Relative light units (RLU) were converted to total adenylate concentrations using a standard curve described previously (*78*). Total nitrogen and carbon % were measured on a CNHS Elemental Analyzer (vario EL cube, Elementar) whereby the total organic carbon % (TOC) was calculated by subtracting the fraction of inorganic carbon from total carbon in the

sample, measured using a calcimeter after acidifying the samples with 10% HCl. The detection limits for TOC and TN were 0.05%.

DNA extraction. We extracted DNA following an established protocol (*38*). In brief, sediments were transferred to 2-mL Lysing Matrix E tubes (MP Biomedicals, Solon, OH, USA) filled with 1.4 mm ceramic spheres, 0.1 mm silica spheres and one 4 mm glass sphere. Lysing buffer was prepared containing (for a 50 mL solution) 4 mL of C1 lysing buffer (MoBio, Carlsbad, CA), 0.8 mL 10% SDS, 7.2 mL 100% ethanol, and 38 mL 1 M disodium hydrogen phosphate (Na_2HPO_4). 1 mL of lysing buffer was added to sediment samples in the tubes, and tubes were homogenized for 40 s in a Fast-Prep 5G homogenizer (MP Biomedicals, Solon, OH, USA) at 6 m/s. After this step, samples were heated for 2 min at 99 °C and then subject to two freeze-thaw cycles. Samples were later centrifuged for 15 min at 4700 rpm at 24 °C, and the supernatant was concentrated in Amicon filters (molecular weight cutoff [MWCO] 50 kDa; Millipore, St. Louis, MO, USA). 100 µL of suspended DNA was later purified using MoBio DNA extraction kit and protocol. DNA concentration was quantified using the Qubit double-stranded DNA high-sensitivity assay kit and a Qubit 3.0 fluorometer (Invitrogen, Eugene, OR, USA). DNA extractions were finally kept at -20 °C for further analyses.

Stable isotope probing incubation setup. Sediment or soil was collected from the surface 2 cm of a 2x2 m area applying the same criteria as for the chronosequence sampling. Approximately 500 g of material was collected in a sterilized plastic sealed bag and SIP incubations were started within 12 hrs of sampling. From sites A, B and C, we incubated 2 g of wet sediment or soil with ^{13}C-labeled amino acids (Sigma-Aldrich, Cat# 767964-1EA), and unlabeled amino acids (Sigma-Aldrich, Cat# 79248-5X2ML) as a control. The amino acid mixture consisted of 17 amino acids (alanine, arginine, aspartic acid, glutamic acid, glycine, histidine, isoleucine, leucine, lysine, methionine, phenylalanine, proline, serine, threonine, tyrosine, valine, and cystine), all of which were supplied at 2.5 mM with the exception of cystine that was supplied in the mixture at 1.25mM. The amino acid mixture was added at a final concentrations of 80 µg g^{-1}, and the samples were incubated in 15-mL Falcon® tubes. We chose to add the amino acids at this concentration because it represents a minor fraction of the naturally existing total organic carbon available to the microbial communities, ca. 0.2-1% and 10-40% of the TOC and TN, respectively (Fig 2a). Adding the amino acid substrates at this concentration was intended to reduce 'tipping the system' away from the naturally low concentrations of TOC but still provide enough ^{13}C-labeled substrate to achieve detectable EAF values in 16S and fungal 18S rRNA genes. Our chosen concentration is within the general concentration range considered to be required for detecting DNA labeling with high-resolution DNA-SIP (*62*), and is similar the concentrations of ^{13}C-labeled amino acids used by previous DNA-SIP studies to trace bacterial carbon assimilation in agricultural soil (*62*) and geothermal soils (*63*).

The addition of the amino acids created a slurry that was gently mixed by pipetting to ensure the substrate was distributed throughout the sediment slurry. Approximately 12 mL of air in the headspace was left to promote aerobic respiration. Tubes were incubated at 4 °C in the dark for either one day or seven days (allowing for two time points) and were terminated by freezing -20 °C. The glacial forefield where the soils and sediments are located is a hydrologically dynamic environment that exposes sediment and soil microbes to large fluctuations in moisture and so the addition of water to the soil and sediment to create a slurry is reflective of natural conditions.

Clay minerals adsorb organic carbon to their surfaces and therefore restrict bioavailability to soil microbes (*74-76*). To test the effect of clay minerals on amino acid assimilation (via sorption), we also

performed SIP incubations with amino acid clay mineral mixtures. We tested two types of clay minerals with varying structures proposed to be important for organic C sorption (*74*, *75*): kaolinite (a 1:1 clay mineral) and montmorillonite (a 2:1 clay mineral). Unlabeled and labeled amino acids were mixed with 20 mg of kaolinite (Sigma-Aldrich) or montmorillonite (Aldrich, K10) in sterile microfuge tubes and incubated for a 15-day pre-incubation prior to the addition to soil incubations, to allow time for amino acids to interact with and potentially sorb to clay mineral surfaces before starting the SIP incubations. The amino acid clay mineral mixtures were added to the soil at the same final concentration of amino acids as the controls that contained no additional clay minerals (80 µg/g amino acids). Tubes were incubated under the same conditions as the controls: at 4 °C in the dark for either one day or seven days (allowing for two time points), after which incubations were terminated by freezing at -20 °C.

Ultracentrifugation and density gradient fractionation. Extracted DNA was prepared for density gradient centrifugation following an established qSIP protocol (*38, 66, 67*). In brief, density gradient centrifugation was performed in a TLN-100 Optima MAX-TL ultracentrifuge (Beckman Coulter, Brea, CA, USA) with a near-vertical rotor at 18°C for 72 h at 165,000 g. In total, 50 µL of extracted DNA was added to a solution of cesium chloride (CsCl) and gradient buffer (0.1 M Tris, 0.1 M KCl, and 1 mM EDTA) in order to achieve a starting density of 1.71 g/mL in 3.3 mL OptiSeal polyallomer tubes (Beckman Coulter, Brea, CA, USA). After ultracentrifugation, density gradients were fractionated into 20 equal fractions of roughly 180 µL from the bottom of OptiSeal polyallomer tubes by using a syringe pump and a fraction recovery system (Beckman Coulter, Brea, CA, USA). Refractive index of the fractions was measured immediately after fraction recovery with an AR200 digital refractometer (Reichert Analytical Instruments, Depew, NY, USA) and converted to density using a standard curve. After measuring the density of the collected fractions, DNA was precipitated overnight at room temperature using 2 volumes of polyethylene glycol with 2 µL (20 mg/mL) glycogen. DNA was pelleted via centrifugation (13,000 g, 40 min), washed with 70% ethanol, and resuspended with 30 µL elution buffer (MoBio DNA extraction kit, Qiagen).

Quantitative PCR of bacterial 16S rRNA genes and fungal 18S rRNA genes. Quantitative PCR (qPCR) was conducted in a CFX Connect real-time PCR system (Bio-Rad, Hercules, CA, USA) as described in detail in a previous publication (*38*). As described previously (*38*), quantification of prokaryotic 16S rRNA genes was done using the primer pair 515F/806R, whereas fungal 18S rRNA genes were quantified using fungal-specific primers FR1 (5'-AICCATTCAATCGGTAIT-3') and FF390 (5'-CGATAACGAACGAGACCT-3') (*79*).

16S rRNA gene and fungal ITS sequencing and analysis. As described previously (*80*), the 16S ribosomal RNA genes of bacteria and archaea were PCR amplified using the primer pair 515F/806R containing dual-indexed primers. The fungal internal transcribed spacer (ITS) was amplified as described previously (*38*), with the primer pair ITS1-F/ITS2 (ITS1-F: 5'-CTTGGTCATTTAGAGGAAGTAA-3', ITS2: 5'-GCTGCGTTCTTCATCGATGC-3') that also contained Illumina adapters and a unique barcode sequence for sample demultiplexing. This was determined to capture a realistic picture of fungal OTU richness using fungal mock communities (*81*). The taxonomic affiliation of the 16S rRNA gene was made as described previously (*80*) using BLASTn searches of OTU sequences against the SILVA database (*83*). The ITS taxonomy was assigned as described previously (*38*) by BLASTn searches of fungal ITS OTUs against the UNITE database release 8 (*84*).

All 16S and ITS1 rRNA gene sequencing data from the chronosequence have been deposited in the NCBI short read archive database under BioProject ID PRJNA1074128. BioProject PRJNA1074128 also includes all the ITS1 sequencing data from the SIP experiments. Namely the ITS1 datasets from each individual density fraction after ultracentrifugation of DNA from ^{13}C-labeled and unlabeled control SIP incubations, which were used for the fungal Tag-SIP and qSIP analyses.

Estimating excess atom ^{13}C-enrichment fraction (EAF) of total 16S and fungal 18S rRNA genes. The excess atom fraction ^{13}C (EAF) was calculated as a measure of the amount of substrate incorporated into DNA of either bacteria or fungi, from the labeled amino acids. The EAF of bacterial 16S rRNA genes and fungal 18S rRNA genes from the labeled amino acid SIP incubations were calculated as previously described (*38*) according to the equations for calculating EAF values from DNA-SIP experiments (*24*). The EAF value should reflect the proportion of labeled carbon atoms that are assimilated into the genomic DNA (or at least large DNA fragments containing rRNA genes). For example, an EAF value of 0.2 would relate to 20% of C atoms within the gene targeted containing the heavier ^{13}C isotope (*24*). When calculating the fungal:bacterial EAF ratio, null results (no detectable labeling) were interpreted as amino acid assimilation being below our EAF detection limit, empirically determined to be 1% (*38*). This allowed us to calculate a F:B EAF ratio in SIP incubations in cases of no detectable amino acid assimilation.

Measuring remineralized ^{13}C from amino acid SIP incubations. To quantify the remineralization of amino acids added to the SIP incubations we determined the relative amount of $^{13}CO_2$ produced using gas chromatography mass spectrometry (GC-MS) of gas withdrawn from the headspace of incubations. Specifically, 0.2 g of incubation material (muddy slurry) was added to 20 mL gas tight glass vials that were crimp sealed with grey butyl stoppers, heated to 60 °C for 5 minutes (in a headspace sampler), and 1 mL of headspace gas was sampled via a headspace autosampler connected to a gas chromatograph with a quadropole mass spectrometer as the detector (GCMS-QP2020 NX, Shimadzu). N_2 was used as the carrier gas. This GC-MS set up is calibrated for trace gas analysis (H_2, CO, CO_2, CH_4), by means of a pre-separation column [U-Bond, 0.32 mm ID, 10 µm Film, 30 m] to separate larger molecules and a second column [Carboxen-1010 Plot, 0.32 mm ID, 15 µm Film, 30 m] for separating trace gases. The elution time for CO_2 on this particular setup (6.1 minutes) was determined by comparison to a CO_2 standard (99.999% Linde Gas). The relative amount of remineralized carbon from the added labeled amino acids was taken as percentage of ^{13}C-labeled CO_2 (m/z = 45) relative to the unlabeled CO_2 (m/z = 44), released from the sample matrix into the flask headspace. These percentages were calculated from the relative abundance of labeled (m/z = 45) and unlabeled (m/z = 44) CO_2, determined via integration of the respective peak areas in the GC-QMS trace. All experimental treatments had $^{13}CO_2$ percentages higher than the corresponding unlabeled control flasks, which consistently reflected the natural abundance of ^{13}C in the environment (1.1% +/- 0.05%).

Estimating ^{13}C assimilation by specific fungal taxa. In order to quantify amino acid assimilation by specific fungal taxa, SIP incubations showing the highest ^{13}C EAF values for fungal 18S rRNA genes (Fig S2) were selected for fungal ITS1 barcoding of the individual density fractions (resulting from density gradient ultracentrifugation). The two samples that were chosen for fungal-specific Tag-SIP and qSIP were the site A control (no mineral addition), and the tundra (+ montmorillonite) incubations at site C, because these represented two end members of the chronosequence which had the highest amount of ^{13}C assimilation as evidenced by the EAF of the fungal 18S rRNA genes (Fig. S2). Due to the extremely low fungal biomass

at site A (Fig. 2c), there was not sufficient material to perform replicates for the site A-control (no mineral addition) incubation. We therefore could not apply the standard qSIP analysis pipeline (*24*) for this SIP incubation. Rather, we used the equations from Hungate *et al.* (*24*) to calculate the excess atom ^{13}C fraction ("A-values") from buoyant density shifts for each individual OTU in the unlabeled incubations relative to the ^{13}C-labeled incubations. We refer to quantifying the excess atom fraction (EAF) for each OTU present in a single sample as quantitative Tag-SIP (*85*), or "Tag-qSIP". Tag-qSIP can be described as pseudo-quantitative, because the relative distribution of ITS1 sequences is quantitatively normalized by the total number of fungal 18S rRNA gene copies determined with qPCR. In the site C (tundra) SIP incubations, the higher fungal biomass was sufficient to perform three replicates for the standard qSIP pipeline. From each incubation fractionation, 12 density fractions in the gradient containing DNA were selected for ITS sequencing following the protocol described above.

The amount of amino acid ^{13}C assimilated by specific fungal taxa was calculated based on an isotopic replacement approach which consists of comparing the buoyant density of DNA for a specific OTU in the treatment with labeled amino acids against a control (*24*). In order to update these calculations for our fungal data, we normalized the fractional sequence abundance of fungal ITS1 OTU sequences using total concentration of fungal 18S rRNA genes (quantified via qPCR) in the same density fractions. We acknowledge that rRNA operon copy numbers vary between fungal taxa (*86*) and may bias fungal EAF comparison between different fungal taxa especially in samples with very different fungal communities. However, this bias should be negligible when comparing EAF of the same fungal OTUs in different samples. The quantitatively normalized fungal ITS1 distributions were then used together with CsCl densities of each fraction, to calculate the average buoyant density of each fungal OTU using the same original equations (*24*) for 16S rRNA genes. These calculations quantify ^{13}C incorporation in the DNA of specific taxa and take into account potential effects of GC content (*24*). The incorporation of the isotope tracer (^{13}C) is expressed as EAF, which represents the increase above the natural abundance isotopic composition and ranges from 0 to 1 minus the natural abundance background (*24*). For the tundra incubations, confidence intervals (CI) of EAF values were calculated as the standard deviation of three replicates (site C). All statistical analyses were performed in R (4.3.1) with RStudio.

Acknowledgements. We acknowledge funding from the Deutsche Forschungsgemeinschaft (DFG) through Project OR 417/7-1 (granted to William D. Orsi), a NSF-NERC (UKRI) thematic program "Signals in the Soil" (NERC grant: NE/T010967/1; NSF grant: 1935689), and NERC COVID Recovery Support Fund. JB also acknowledges support from the CNRS Chaires de Professeur Junior (CPJ). We are grateful to the staff of the UK Arctic Research Station and the Ny-Ålesund Research Station – Sverdrup, in Ny-Ålesund, Svalbard, for logistical support in the field. A part of the research was performed in the scope of the Master Program "Geobiology and Paleobiology" (MGAP) at LMU Munich (https://www.mgap.geo.uni-muenchen.de/index.html). We acknowledge the SUN SPEARS 2021 field team and investigators (Trevor P. Irons, Carlos Oroza, Oliver Kuras, Mihai Cimpoiasu, Harry Harrison, Dane Liljestrand, Justin Byington, Michael Jarzin) for assistance in the field and with funding acquisition.

Author contributions

WDO, JB, and JC conceived the idea for the study. WDO, JB, PS and SKS obtained funding. JC, JB, SKS, and PS obtained samples. JC and JP conducted experiments and produced data. JC, JP, and WDO analyzed

data. JC, JB, and WDO wrote the paper. WDO and JB supervised the study. All co-authors provided comments on the manuscript and participated in the editing process.

Competing interests

The authors declare no competing interests.

Figure legends

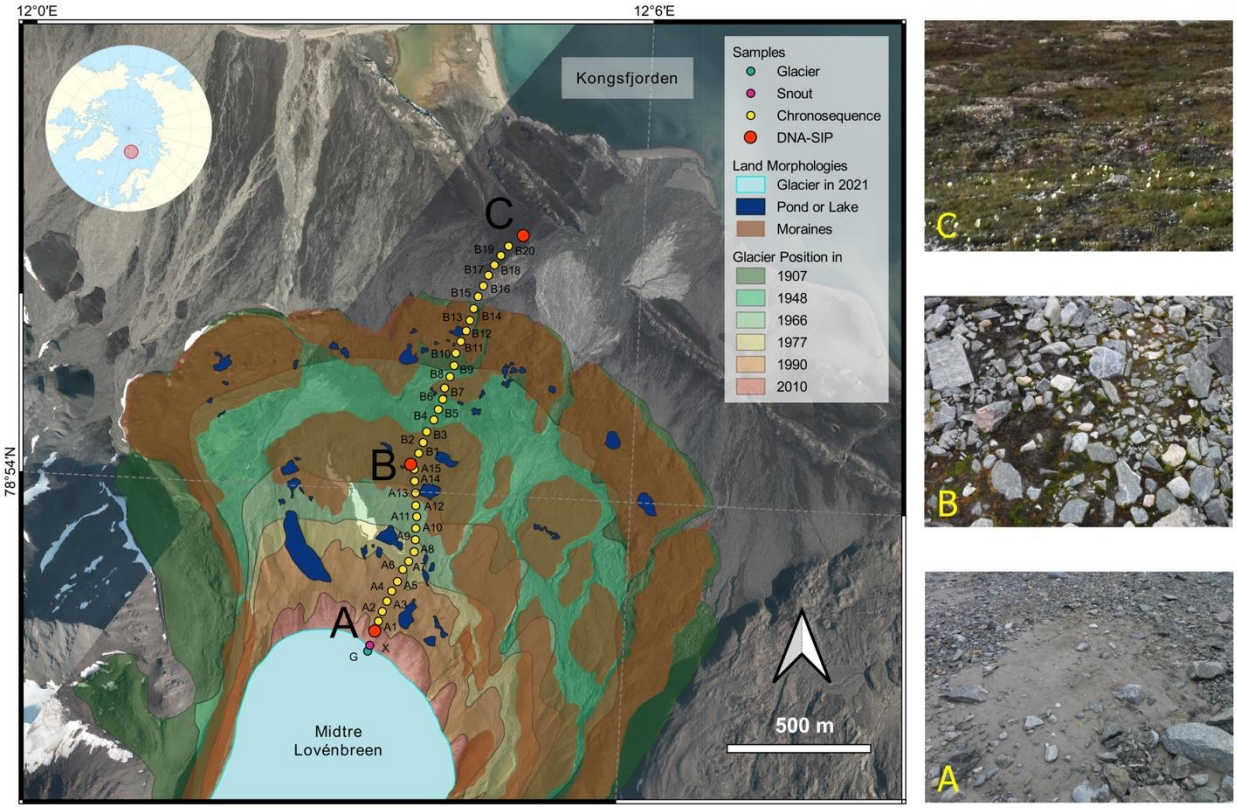

Figure 1. Aerial view of the Midtre Lovénbreen glacier forefield and chronosequence sampling transect showing locations for SIP incubations. The photo of Midtre Lovénbreen's forefield on the West coast of Spitsbergen, Svalbard, is a satellite image from the Norwegian Polar Institute. Glacier front lines and their respective ages over the last century were obtained from the published estimates of Bourriquen *et al.* (2018) according to the Norwegian Polar Institute data. **Right:** Photographs of sites A (proglacial rock flour sediment), B (rocky, intermediate soils) and C (developed tundra soils) where the stable isotope probing (SIP) incubations were performed.

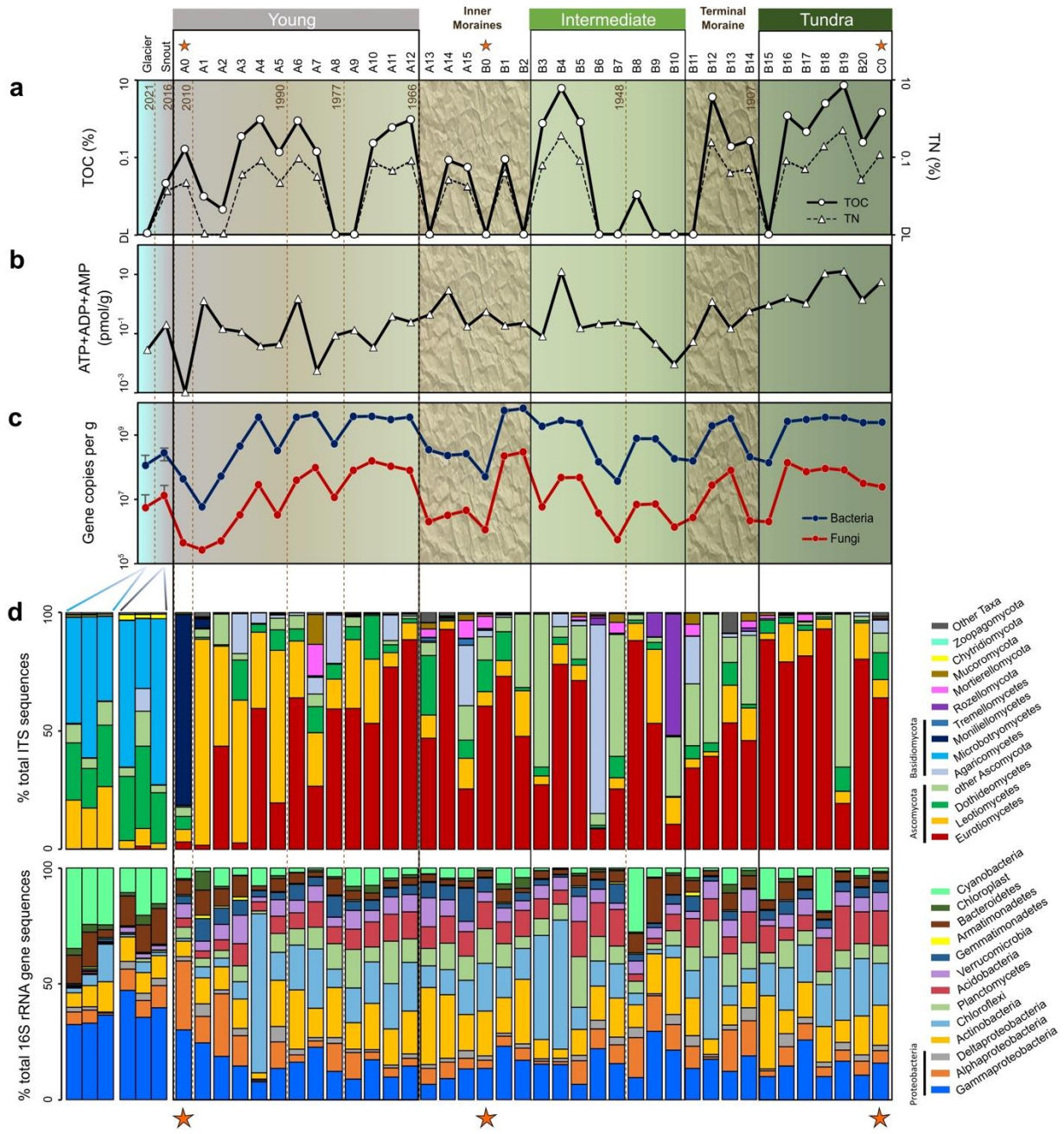

Figure 2. Biomass accumulation and microbial community assembly across a 100-yr soil Arctic proglacial soil chronosequence. a: Total organic carbon (TOC) and total nitrogen (TN) concentrations. The detection limit for TOC and TN was 0.001 %. DL: detection limit. **b:** Total adenylate (ATP+ADP+AMP) concentration. **c:** Concentrations of bacterial 16S (blue) and fungal 18S (red) rRNA gene copies. **d:** Relative abundance of major taxonomic groups within 16S rRNA gene and fungal ITS datasets. For the glacier and snout, three replicates were taken and are displayed at the left of the chronosequence. The orange stars indicate the sites where SIP incubations were conducted. Glacier front lines, their respective ages over the last century, were obtained from the published estimates of Bourriquen *et al.* (2018) according to the Norwegian Polar Institute data.

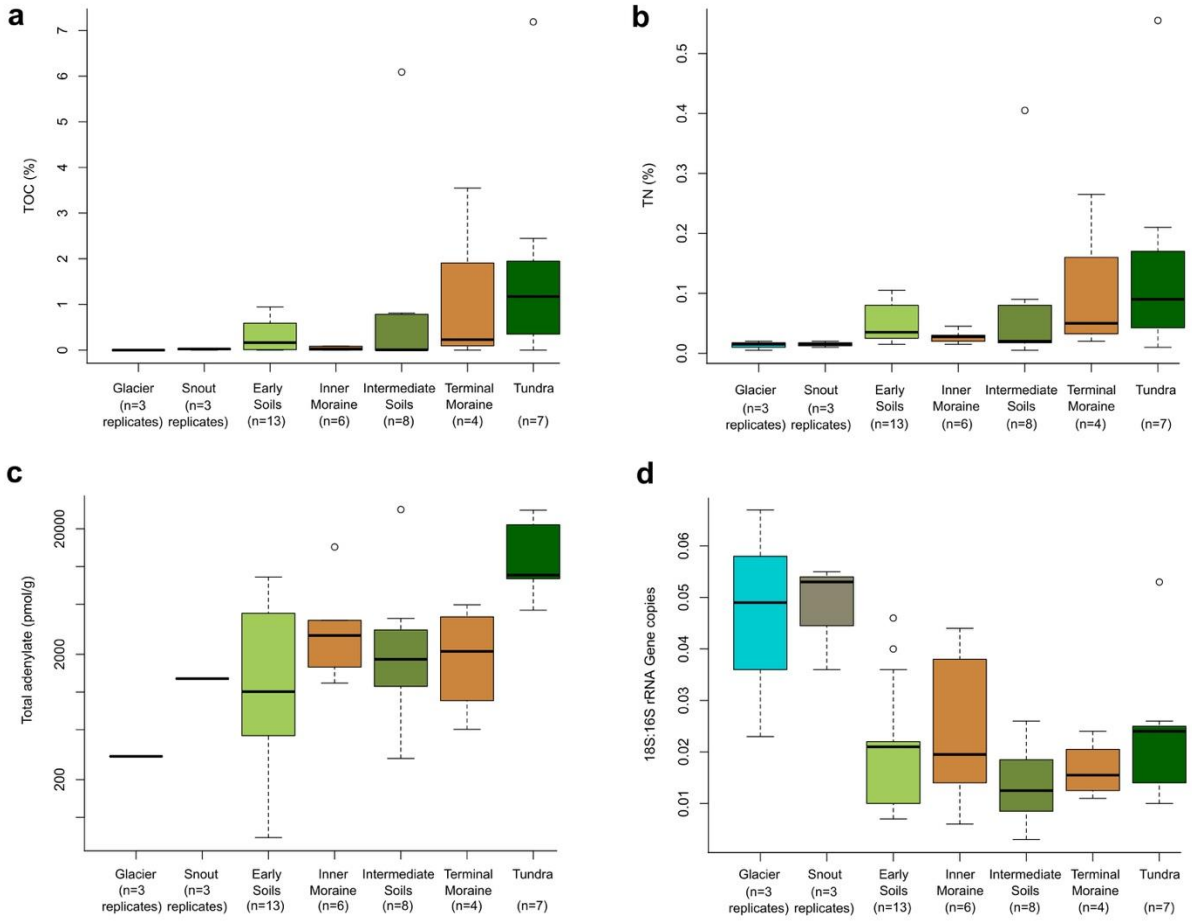

Figure 3. Boxplots of soil biochemistry and microbial biomass by soil succession stage. a. Total organic carbon concentrations (TOC %) **b.** Total nitrogen concentrations (TN %). **c.** Total adenylate concentrations (ATP+ADP+AMP). **d.** F:B ratios based on qPCR quantification of rRNA gene concentrations (fungal 18S:16S). The samples are derived from a single transect and grouped into the gradient classes based on age-estimates and large-scale geomorphological features (see Fig. 1). The glacier and snout classes had three biological replicates, whereas all other groups derive from single samples along the transect grouped into geomorphological features.

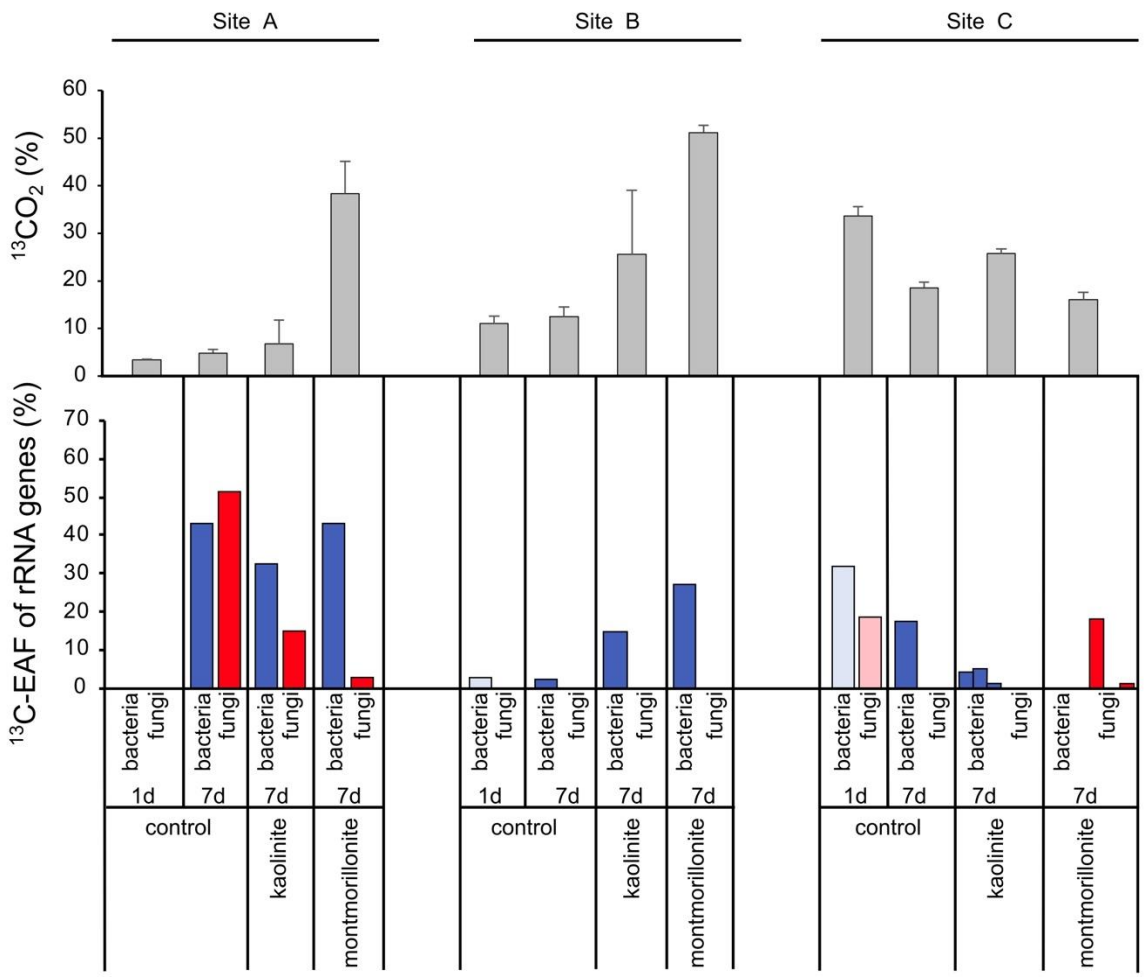

Figure 4. Fungal ^{13}C excess atomic fraction (^{13}C-EAF), bacterial ^{13}C-EAF, and ^{13}C-labeled CO_2 production across the chronosequence. Top panel: The percentage of ^{13}C-labeled CO_2 at the end of the SIP incubations. Shaded bars and error bars represent average and standard deviations from three technical replicates. **Bottom panel:** ^{13}C-EAF values for fungal 18S (red) and bacterial 16S (blue) rRNA genes. Control: ^{13}C-labeled amino acid addition with no added clay minerals. Kaolinite: ^{13}C-labeled amino acids supplemented with kaolinite. Montmorillonite: ^{13}C-labeled amino acids supplemented with montmorillonite. At the tundra site C, three technical replicates for DNA density gradient fractionation were performed for the kaolinite and montmorillonite stable isotope probing (SIP) incubations that are represented by three individual bars.

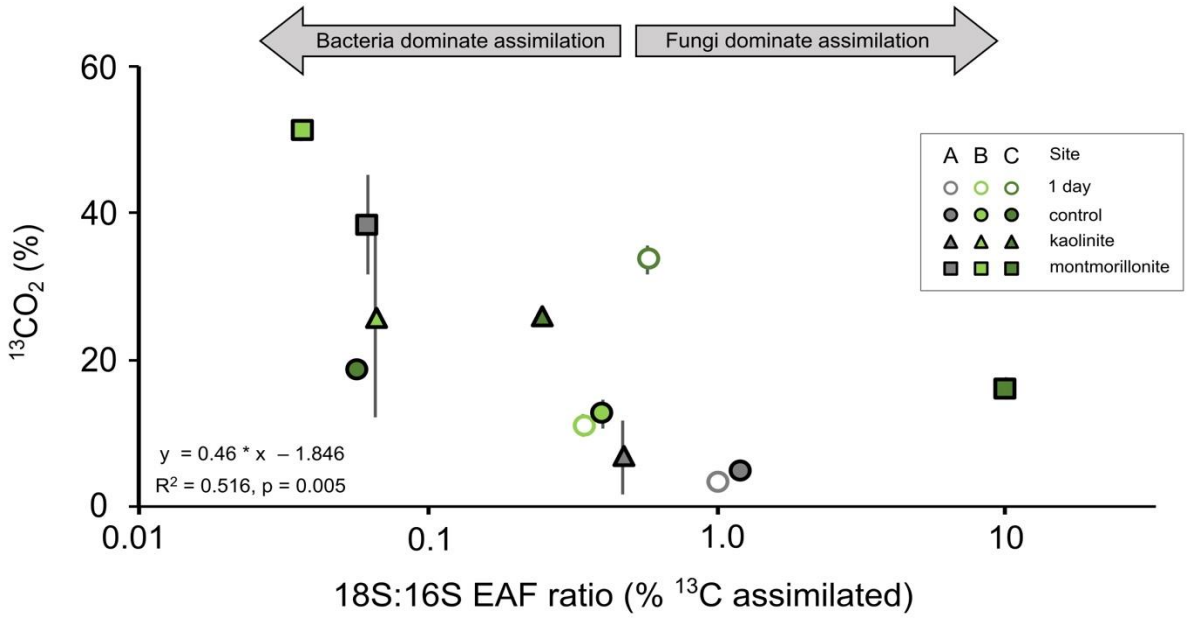

Figure 5. Remineralized $^{13}CO_2$ as a function of the fungal:bacterial (18S:16S) ^{13}C excess atomic fraction (^{13}C-EAF) ratio. The x axis represents the ratio of fungal 18S rRNA ^{13}C-EAF compared to the bacterial 16S rRNA ^{13}C-EAF in the respective ^{13}C-labeled amino acid SIP incubations. The y axis indicates the % of CO_2 that contained the ^{13}C label, error bars represent standard deviations. Open circles represent 1 day SIP incubations (^{13}C-labeled amino acid incubations with no clay minerals added). Filled symbols represent 7 days stable isotope probing (SIP) incubations. Circles: ^{13}C-labeled amino acid with no clay minerals added, triangles: ^{13}C-labeled amino acids with additional kaolinite, squares: ^{13}C-labeled amino acids with additional montmorillonite. Note than increased F:B ^{13}C-EAF ratios is correlated with decreased $^{13}CO_2$ production.

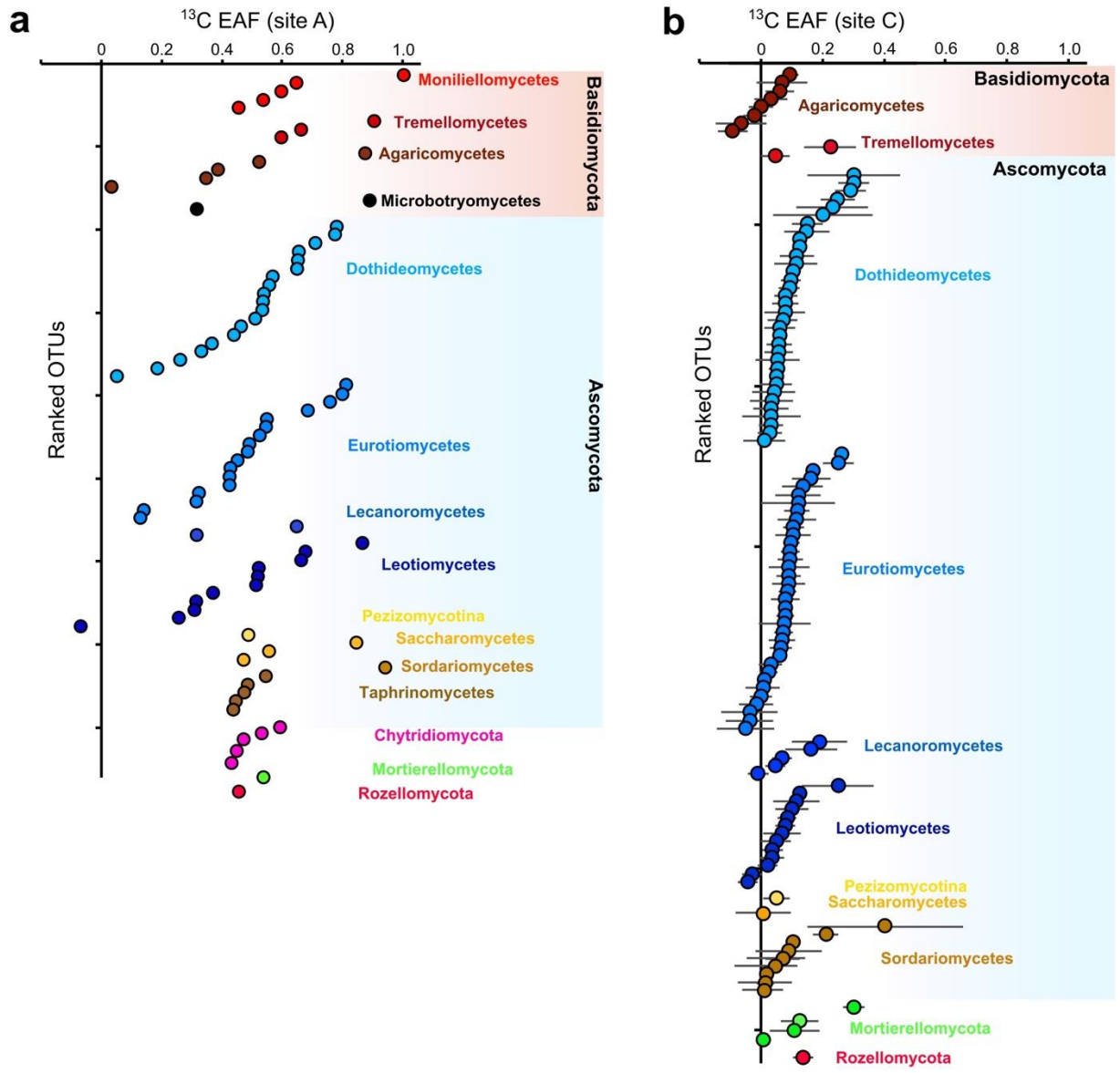

Figure 6. ^{13}C excess atomic fraction (^{13}C-EAF) values for specific fungal taxa in proglacial sediments (panel a) and Arctic tundra (panel b). Individual points represent fungal OTUs and their respective ^{13}C-EAF values are represented by the x axis. For the tundra sample, bars correspond to the standard deviation across three DNA density gradient fractionation replicates (technical replicates) from the stable isotope probing (SIP) incubation.

References

1. R. Hugonnet, R. McNabb, E. Berthier, B. Menounos, C. Nuth, L. Girod, D. Farinotti, M. Huss, I. Dussaillant, F. Brun, A. Kääb, Accelerated global glacier mass loss in the early twenty-first century. *Nature* **592**, 726-731 (2021).
2. R. V. Bekryaev, I. V. Polyakov, V. A. Alexeev, Role of polar amplification in long-term surface air temperature variations and modern arctic warming. *J. Clim.* **23**, 3888-3906 (2010).
3. F. Pithan, T. Mauritsen, Arctic amplification dominated by temperature feedbacks in contemporary climate models. *Nature Geoscience* **7**, 181-184 (2014).
4. B. Noel *et al.*, Low elevation of Svalbard glaciers drives high mass loss variability. *Nat Commun* **11**, 4597 (2020).
5. S. Yoshitake, M. Uchida, Y. Iimura, T. O'htsuka, T. Nakatsubo, Soil microbial succession along a chronosequence on a High Arctic glacier foreland, Ny-Ålesund, Svalbard: 10 years' change. *Polar Science* **16**, 59-67 (2018).
6. S. Cauvy-Fraunie, O. Dangles, A global synthesis of biodiversity responses to glacier retreat. *Nat Ecol Evol* **3**, 1675-1685 (2019).
7. R. Wojcik, J. Eichel, J. A. Bradley, L. G. Benning, How allogenic factors affect succession in glacier forefields. *Earth-Science Reviews* **218**, 103642 (2021).
8. S. P. Brown, A. Jumpponen, Contrasting primary successional trajectories of fungi and bacteria in retreating glacier soils. *Mol Ecol* **23**, 481-497 (2014).
9. J. A. Bradley, J. S. Singarayer, A. M. Anesio, Microbial community dynamics in the forefield of glaciers. *Proc Biol Sci* **281**, (2014).
10. S. K. Schmidt *et al.*, The earliest stages of ecosystem succession in high-elevation (5000 metres above sea level), recently deglaciated soils. *Proc Biol Sci* **275**, 2793-2802 (2008).
11. F. D. Alfaro *et al.*, Soil microbial abundance and activity across forefield glacier chronosequence in the Northern Patagonian Ice Field, Chile. *Arctic, Antarctic, and Alpine Research* **52**, 553-562 (2020).
12. S. K. Schmidt *et al.*, Biogeochemical stoichiometry reveals P and N limitation across the post-glacial landscape of Denali National Park, Alaska. *Ecosystems* **19**, 1164-1177 (2016).
13. J. L. Darcy *et al.*, Phosphorus, not nitrogen, limits plants and microbial primary producers following glacial retreat. *Sci Adv* **4**, eaaq0942 (2018).
14. S. C. Castle *et al.*, Nutrient limitation of soil microbial activity during the earliest stages of ecosystem development. *Oecologia* **185**, 513-524 (2017).
15. G. Varliero, A. M. Anesio, G. L. Barker, A taxon-wise insight into rock weathering and nitrogen fixation functional profiles of proglacial systems. *Frontiers in Microbiology* **12**, 627437 (2021).
16. J. Knelman, S. K. Schmidt, G. E. B., Cyanobacteria in early soil development of deglaciated forefields: Dominance of non-heterocystous filamentous cyanobacteria and phosphorus limitation of N-fixing Nostocales. *Soil Biol Biochem* **154**, 108127 (2021).
17. I. D. Hodkinson, S. J. Coulson, N. R. Webb, Community assembly along proglacial chronosequences in the high Arctic: vegetation and soil development in north-west Svalbard. . *Journal of Ecology* **91**, 651-663 (2003).
18. J. A. Bradley, in *Microbial Life in the Cryosphere and its Feedback on Global Change,* S. Liebner, L. Ganzert, Eds. (de Gruyter, Berlin, Boston, 2021), pp. 253-264.

19. P. F. Hoffman *et al.*, Snowball Earth climate dynamics and Cryogenian geology-geobiology. *Sci Adv* **3**, e1600983 (2017).
20. G. Gleixner, Soil organic matter dynamics: a biological perspective derived from the use of compound-specific isotopes studies. *Ecol. Res.* **28**, 683–695 (2013).
21. J. P. Schimel, S. M. Schaeffer, Microbial control over carbon cycling in soil. *Front. Microbiol.* **3**, 348 (2012).
22. F. Tao *et al.*, Microbial carbon use efficiency promotes global soil carbon storage. *Nature* **618**, 981-985 (2023).
23. P. Dijkstra *et al.*, Modeling soil metabolic processes using isotopologue pairs of position-specific 13CC-labeled glucose and pyruvate. *Soil Biol Biochem* **43**, 1848-1857 (2011).
24. B. A. Hungate *et al.*, Quantitative microbial ecology through stable isotope probing. *Appl Environ Microbiol* **81**, 7570-7581 (2015).
25. Y. Sakata-Bekku, T. Nakatsubo, A. Kume, H. Koizumi, Soil microbial biomass, respiration rate, and temperature dependence on a successional glacier foreland in Ny-Ålesund, Svalbard. *Arctic, Antarctic, and Alpine Research* **34**, 395-399 (2004).
26. K. K. Treseder, J. T. Lennon, Fungal traits that drive ecosystem dynamics on land. *Microbiol Mol Biol Rev* **79**, 243-262 (2015).
27. A. A. Malik *et al.*, Soil Fungal:Bacterial Ratios Are Linked to Altered Carbon Cycling. *Front Microbiol* **7**, 1247 (2016).
28. M. S. Strickland, J. Rousk, Considering fungal:bacterial dominance in soils – Methods, controls, and ecosystem implications. *Soil Biol Biochem* **42**, 1385-1395 (2010).
29. R. L. Sinsabaugh, S. Manzoni, D. L. Moorehead, A. Richter, Carbon use efficiency of microbial communities: stoichiometry, methodology and modelling. *Ecol. Lett.* **16**, 930-939 (2013).
30. J. Fabian, S. Zlatanovic, M. Mutz, K. Premke, Fungal-bacterial dynamics and their contribution to terrigenous carbon turnover in relation to organic matter quality. *ISME J* **11**, 415-425 (2017).
31. V. L. Bailey, J. L. Smith, H. Bolton, Fungal-to-bacterial ratios in soils investigated for enhanced C sequestration. *Soil Biol Biochem* **34**, 997-1007 (2002).
32. R. D. Bardgett, P. J. Hobbs, Å. Frostegård, Changes in soil fungal:bacterial biomass ratios following reductions in the intensity of management of an upland grassland. *Biol. Fertil. Soils* **22**, 261-264 (1996).
33. J. Six, S. D. Frey, R. K. Thiet, K. M. Batten, Bacterial and fungal contributions to carbon sequestration in agroecosystems. *Soil Sci. Soc. Am. J.* **70**, 555-569 (2006).
34. B. G. Waring, C. Averill, C. Hawkes, Differences in fungal and bacterial physiology alter soil carbon and nitrogen cycling: insights from meta-analysis and theoretical models. *Ecol. Lett.* **16**, 887-894 (2013).
35. V. de Garcia, S. Brizzio, D. Libkind, P. Buzzini, M. van Broock, Biodiversity of cold-adapted yeasts from glacial meltwater rivers in Patagonia, Argentina. *FEMS Microbiol Ecol* **59**, 331-341 (2007).
36. P. Dresch *et al.*, Emerging from the ice-fungal communities are diverse and dynamic in earliest soil developmental stages of a receding glacier. *Environ Microbiol* **21**, 1864-1880 (2019).
37. L. Tedersoo *et al.*, Fungal biogeography. Global diversity and geography of soil fungi. *Science* **346**, 1256688 (2014).
38. W. D. Orsi *et al.*, Carbon assimilating fungi from surface ocean to subseafloor revealed by coupled phylogenetic and stable isotope analysis. *ISME J* **16**, 1245-1261 (2022).

39. P. L. Sorensen, A. Michelsen, I. Jonassen, Ecosystem partitioning of 15N-glycine after long-term climate and nutrient manipulations, plant clipping and addition of labile carbon in a subarctic heath tundra. *Soil Biol Biochem* **40**, 2344-2350 (2008).
40. J. Hobbie, J. Hobbie, Amino acid cycling in plankton and soil microbes studied with radioisotopes: measured amino acids in soil do not reflect bioavailability. *Biogeochemistry* **107**, 339-360 (2012).
41. A. Nordin, I. K. Schmidt, G. R. Shaver, Nitrogen uptake by arctic soil microbes and plants in relation to soil nitrogen supply. *Ecology* **85**, 995-962 (2004).
42. B. G. Pautler *et al.*, Molecular characterization of dissolved organic matter in glacial ice: coupling natural abundance 1H NMR and fluorescence spectroscopy. *Environ Sci Technol* **46**, 3753-3761 (2012).
43. M. Kida *et al.*, Dissolved Organic Matter Processing in Pristine Antarctic Streams. *Environ Sci Technol* **55**, 10175-10185 (2021).
44. J. Bradley *et al.*, Microbial dynamics in a High-Arctic glacier forefield: a combined field, laboratory, and modelling approach. *Biogeosciences* **13**, 5677-5696 (2016).
45. S. Yoshitake, M. Uchida, H. Koizumi, T. Nakatsubo, Carbon and nitrogen limitation of soil microbial respiration in a High Arctic successional glacier foreland near Ny-Ålesund, Svalbard. . *Polar Research* **26**, 22-30 (2007).
46. Y. Liu *et al.*, Plant colonization mediates the microbial community dynamics in glacier forelands of the Tibetan Plateau. *iMeta* **2**, e91 (2023).
47. F. A. Thomas, R. K. Sinha, K. P. Krishnan, Bacterial community structure of a glacio-marine system in the Arctic (Ny-Ålesund, Svalbard). *Sci Total Environ* **20**, 135264 (2020).
48. W. Hu, S. K. Schmidt, P. Sommers, J. L. Darcy, D. L. Porazinska, Multiple-trophic patterns of primary succession following retreat of a high-elevation glacier. *Ecosphere* **12**, e03400 (2021).
49. C. L. Schoch *et al.*, Nuclear ribosomal internal transcribed spacer (ITS) region as a universal DNA barcode marker for Fungi. *PNAS* **16**, (2012).
50. R. A. Duo Saito *et al.*, Metabarcoding analysis of the fungal biodiversity associated with Castaño Overa glacier – Mount Tronador, Patagonia, Argentina. *Fungal Ecology* **36**, 8-16 (2018).
51. L. Perini, K. Andrejasic, C. Gostincar, N. Gunde-Cimerman, P. Zalar, Greenland and Svalbard glaciers host unknown basidiomycetes: the yeast Camptobasidium arcticum sp. nov. and the dimorphic Psychromyces glacialis gen. and sp. nov. *Int J Syst Evol Microbiol* **71**, (2021).
52. L. Perini *et al.*, Darkening of the Greenland Ice Sheet: Fungal Abundance and Diversity Are Associated With Algal Bloom. *Front Microbiol* **10**, 557 (2019).
53. L. Perini, C. Gostincar, N. Gunde-Cimerman, Fungal and bacterial diversity of Svalbard subglacial ice. *Sci Rep* **9**, 20230 (2019).
54. P. Buzzini, M. Turk, L. Perini, B. Turchetti, N. Gunde-Cimerman, in *Yeasts in Natural Ecosystems,* P. Buzzini, M. A. Lachance, A. Yurkov, Eds. (Springer, Cham, 2017), pp. 331-365.
55. A. Edwards *et al.*, A distinctive fungal community inhabiting cryoconite holes on glaciers in Svalbard. *Fungal Ecology* **6**, 168-176 (2013).
56. B. Luo *et al.*, Habitat-specificity and diversity of culturable cold-adapted yeasts of a cold-based glacier in the Tianshan Mountains, northwestern China. *Appl Microbiol Biotechnol* **103**, 2311-2327 (2019).
57. V. de Garcia, P. Zalar, S. Brizzio, N. Gunde-Cimerman, M. van Broock, Cryptococcus species (Tremellales) from glacial biomes in the southern (Patagonia) and northern (Svalbard) hemispheres. *FEMS Microbiol Ecol* **82**, 523-539 (2012).

58. C. Coleine, J. E. Stajich, L. Selbmann, Fungi are key players in extreme ecosystems. *Trends Ecol Evol* **37**, 517-528 (2022).
59. J. Tian *et al.*, Ecological Succession Pattern of Fungal Community in Soil along a Retreating Glacier. *Front Microbiol* **8**, 1028 (2017).
60. P. Vinšová *et al.*, The biogeochemical legacy of arctic subglacial sediments exposed by glacier retreat. *Global Biogeochem Cycles* **36**, e2021GB007126 (2022).
61. J. A. Bradley *et al.*, Active and dormant microorganisms on glacier surfaces. *Geobiology* **21**, 244-261 (2023).
62. I. J. Klarenberg, C. Keuschnig, A. Salazar, L. G. Benning, O. Vilhelmsson, Moss and underlying soil bacterial community structures are linked to moss functional traits. *Ecosphere* **14**, e4447 (2023).
63. S. E. Barnett, N. D. Youngblut, C. N. Koechli, D. H. Buckley, Multisubstrate DNA stable isotope probing reveals guild structure of bacteria that mediate soil carbon cycling. *Proc Natl Acad Sci U S A* **118**, (2021).
64. D. Lai *et al.*, Resource partitioning and amino acid assimilation in a terrestrial geothermal spring. *ISME J* **17**, 2112-2122 (2023).
65. A. L. Robinson, N. Deluigi, C. Rolland, N. Manetti, T. Battin, Glacier loss and vegetation expansion alter organic and inorganic carbon dynamics in high-mountain streams. *Biogeosciences* **20**, 2301-2316 (2023).
66. O. K. Coskun *et al.*, Quantifying the effects of hydrogen on carbon assimilation in a seafloor microbial community associated with ultramafic rocks. *ISME J* **16**, 257-271 (2022).
67. O. K. Coskun *et al*., Quantifying genome specific carbon fixation in a 750 meter deep subsurface hydrothermal microbial community. *FEMS Microbiology Ecology* **fiae062**, doi.org/10.1093/femsec/fiae062 (2024).
68. G. S. de Hoog, *The Black Yeasts, II: Moniliella and Allied Genera*. Studies in mycology; no. 19 (Centraalbureau voor Schimmelcultures, 1979).
69. C. A. Rosa *et al.*, Synonymy of the yeast genera Moniliella and Trichosporonoides and proposal of Moniliella fonsecae sp. nov. and five new species combinations. *Int J Syst* **59**, doi.org/10.1099/ijs.0.065117-0 (2009).
70. G. S. de Hoog, M. T. Smith, C. A. Rosa, in *The Yeasts,* C. P. Kurtzman, J. W. Fell, T. Boekhout, Eds. (Elsevier, 2011), pp. 1837-1846.
71. S. Ruisi, D. Barreca, L. Selbmann, L. Zucconi, S. Onofri, Fungi in Antarctica. *Rev. Environ. Sci. Biotechnol* **6**, 127-141.
72. F. Maillard, *et al*., Melanization slows the rapid movement of fungal necromass carbon and nitrogen into both bacterial and fungal decomposer communities and soils. *mSystems* **8**, e0039023 (2023).
73. S. R. Thomas-Hall *et al.*, Cold-adapted yeasts from Antarctica and the Italian Alps-description of three novel species: Mrakia robertii sp. nov., Mrakia blollopis sp. nov. and Mrakiella niccombsii sp. nov. *Extremophiles* **14**, 47-59 (2010).
74. M. Kleber *et al.*, Dynamic interactions at the mineral–organic matter interface. *Nature Reviews Earth & Environment* **2**, 402-421 (2021).
75. J. D. Hemingway *et al.*, Mineral protection regulates long-term global preservation of natural organic carbon. *Nature* **570**, 228-231 (2019).

76. W. Szymański et al., Occurrence and stability of organic intercalation in clay minerals from permafrost-affected soils in the High Arctic–A case study from Spitsbergen (Svalbard). Geoderma 408, 115591 (2022).
77. M. Bourriquen *et al.*, Paraglacial coasts responses to glacier retreat and associated shifts in river floodplains over decadal timescales *Land Degradation & Development* **29**, 4173-4185 (2018).
78. W. D. Orsi, A rapid method for measuring ATP + ADP + AMP in marine sediment. *Environ Microbiol* **25**, 1549-1558 (2023).
79. N. Chemidlin Prevost-Boure *et al.*, Validation and application of a PCR primer set to quantify fungal communities in the soil environment by real-time quantitative PCR. *PLoS One* **6**, e24166 (2011).
80. M. Pichler *et al.*, A 16S rRNA gene sequencing and analysis protocol for the Illumina MiniSeq platform. *Microbiologyopen* **7**, e00611 (2018).
81. A. S. Ortega-Arbulu, M. Pichler, A. Vuillemin, W. D. Orsi, Effects of organic matter and low oxygen on the mycobenthos in a coastal lagoon. *Environ Microbiol* **21**, 374-388 (2019).
82. R. C. Edgar, UPARSE: highly accurate OTU sequences from microbial amplicon reads. *Nat Methods* **10**, 996-998 (2013).
83. C. Quast *et al.*, The SILVA ribosomal RNA gene database project: improved data processing and web-based tools. *Nucleic Acids Res* **41**, D590-596 (2013).
84. R. H. Nilsson *et al.*, The UNITE database for molecular identification of fungi: handling dark taxa and parallel taxonomic classifications. *Nucleic Acids Res* **47**, D259-D264 (2019).
85. W. D. Orsi *et al.*, Diverse, uncultivated bacteria and archaea underlying the cycling of dissolved protein in the ocean. *ISME J* **10**, 2158-2173 (2016).
86. L. A. Lofgren, J. K. Uehling, S. Branco, T. D. Bruns, F. Martin, P. G. Kennedy, Genome-based estimates of fungal rDNA copy number variation across phylogenetic scales and ecological lifestyles. *Molecular Ecology* **28**, 721-730 (2018).